

# Temperature gradient driven short wavelength modes in sheared slab plasmas

Zhe Gao<sup>a)</sup>

*Department of Engineering Physics, Tsinghua University, Beijing 100084, People's Republic of China*

H. Sanuki and K. Itoh

*National Institute for Fusion Science, Toki, Gifu 509-5292, Japan*

J. Q. Dong

*Southwestern Institute of Physics, Chengdu 610041, People's Republic of China*

(Received 6 March 2003; accepted 23 April 2003)

The temperature gradient ( $\eta_i$  and  $\eta_e$ ) driven instability in the short wavelength regime,  $|k_y \rho_i| > 1$ , is studied in a sheared slab. An analytical analysis is performed first to clarify the physics mechanisms for the modes in a shearless slab. The correlation between the growth rate and the real frequency of the modes is discussed in detail. The electron temperature gradient is found to have strong influences on the modes in short wavelength regions. Several series of the short wavelength modes are then identified with a kinetic integral equation code in a sheared slab. The radial widths of the modes are found to be comparable with the conventional  $\eta_i$  modes and not short, although the poloidal wavelengths are short. The lowest odd mode usually dominates in the weak magnetic shear and low  $\beta$  regime. However, the fundamental mode seems to be important in tokamak plasmas because the higher order modes are easily stabilized by finite  $\beta$  and/or by magnetic shear. The fundamental short wavelength mode cannot be stabilized by  $\beta$  when the magnetic gradient drift effect is taken into account. The modes are excited by both finite  $\eta_i$  and  $\eta_e$ , and may be stabilized by magnetic shear. © 2003 American Institute of Physics. [DOI: 10.1063/1.1583712]

## I. INTRODUCTION

Understanding the anomalous transport in magnetically confined plasmas has been one of the major challenges for magnetic confinement fusion research for decades. It is now widely accepted that the anomalous transport is induced by turbulent plasma fluctuations with small scales, the so-called microinstabilities.<sup>1</sup> In particular, the temperature gradient (TG) driven instabilities are proposed as the plausible candidates responsible for anomalous thermal transport and have been studied extensively.<sup>2–11</sup> Recent experiments have shown that ion thermal diffusivity reduces to the neoclassical level in improved confinement tokamak plasmas.<sup>12,13</sup> This transport reduction is explained by the model based on the  $\mathbf{E} \times \mathbf{B}$  shear suppression effects on the ion temperature gradient (ITG) turbulence, since the measured  $\mathbf{E} \times \mathbf{B}$  shearing rate exceeds the maximum linear growth rate of the ITG mode.<sup>14–16</sup> Also, nonlinear structures of zonal flows<sup>17</sup> and/or streamers<sup>18</sup> are generated to regulate the turbulent transport. However, the electron transport is often still anomalous even in discharges with an internal transport barrier (ITB). It was observed in the Joint European Torus that after the formation of an ITB, long wavelength modes are suppressed, while short wavelength modes are not.<sup>19</sup> The anomalous electron transport is possibly attributable to short wavelength modes.

The electron temperature gradient (ETG) mode in the electron diamagnetic direction ( $\omega_r > 0$ ) is unstable in the very short wavelength regime  $k_y \rho_e \sim 1$ . Therefore, numerous studies have been performed on the ETG instabilities in recent years.<sup>20–22</sup> However, another unstable mode driven by

temperature gradients in the short wavelength regime  $|k_y \rho_i| \gg 1$  was recently identified by Smolyakov *et al.*<sup>23</sup> This mode propagates in the ion diamagnetic direction ( $\omega_r < 0$ ) and seems to be a continuous extension of the conventional ( $|k_y \rho_i| \sim 1$ ) ITG mode. In fact, in an early study of the local ITG mode, Pu and Migliuolo<sup>24</sup> had pointed out the “double-humped” behavior, with one peak of the growth rate in the regime  $|k_y \rho_i| < 1$  and another peak in the regime  $|k_y \rho_i| \gg 1$ . This behavior was explained to be attributable to the non-monotonic behavior of the real frequency as the cross-field wavelength varies. So, the issue that needs to be clarified is the relation between the “double-humped” behavior in Pu and Migliuolo<sup>24</sup> and the new short wavelength mode discussed by Smolyakov *et al.*<sup>23</sup>

Hirose *et al.*<sup>25</sup> also indicate the existence of a temperature gradient driven mode in the short wavelength regime using a kinetic electromagnetic integral code. The mode propagates in the ion diamagnetic direction and requires both finite  $\eta_i$  and  $\eta_e$  for excitation. The study is performed in the toroidal geometry, but trapped electrons and toroidicity do not seem essential for this mode. Therefore, it may be easier to identify and to investigate the modes in more detail, e.g., whether other unstable modes exist in the short wavelength regime, how the electron kinetics influences the mode, etc., in a sheared slab.

In this paper, we first confirm the explanation in Pu and Migliuolo<sup>24</sup> for the short wavelength temperature gradient modes. The growth rate hump in the short wavelength regime in Pu and Migliuolo<sup>24</sup> is much slighter than that in Smolyakov *et al.*<sup>23</sup> only due to different  $\eta_e$  and  $k_{\parallel}$ . This local short wavelength mode is just attributable to the Lan-

<sup>a)</sup>Electronic mail: gaozhe@mail.tsinghua.edu.cn

dau damping/inverse Landau damping mechanism and the nonmonotonic behaviors of the real frequencies as the wavelength varies. In addition, we also find that the electron kinetics strongly influences the properties of the mode in the short wavelength regime. The mode displays various kinds of behaviors for choice of different  $\eta_e$ . It is stable in the very short wavelength regime  $k_y \rho_e > 1$  when  $\eta_e$  is very small ( $\ll 1$ ) or larger than  $\eta_i$ .

The integral equation for the study of ITG modes in arbitrary  $\beta$  plasmas<sup>26</sup> is upgraded and employed for the nonlocal study of short wavelength modes in a sheared slab in this work. We found other eigenmodes in the short wavelength regime. For typical tokamak parameters the short wavelength mode under consideration is separated from the conventional ITG mode. However, when  $\beta$  or  $\eta_e$  is increased, the coupling between the short wavelength mode and the conventional mode occurs. The coupling results in a continuous  $k_y$  spectrum from the long wavelength regime to the short wavelength regime. Similar to what is found in Hirose *et al.*,<sup>25</sup> the short wavelength modes require both finite  $\eta_i$  and  $\eta_e$ . However, the magnetic shear stabilizes the short wavelength modes, that is not shown in Hirose *et al.*<sup>25</sup>

The organization of this paper is as follows. The updated integral equations are presented in Sec. II. The local results and analyses are described in Sec. III. The nonlocal results are given in Sec. IV. Section V is devoted to conclusions.

## II. ELECTROMAGNETIC INTEGRAL EQUATION FORMALISM

We consider a sheared magnetic field  $\mathbf{B} = B_0[\hat{z}(1 + x/L_B) + \hat{y}(x/L_s)]$ , where  $L_s$  and  $L_B$  are the scale lengths of the magnetic shear and the magnetic gradient, respectively. The static equilibrium in a high  $\beta$  plasma slab requires a magnetic gradient,  $L_n/L_B = \sum_{j=i,e}(\beta_j/2)(1 + \eta_j)$ . Here,  $L_n^{-1} = -(1/n_j)dn_j/dx$ ,  $\eta_j = d \ln T_j/d \ln n_j$  and  $\beta_j = 8\pi n_j T_j/B^2$ . The equilibrium distributions for ions and electrons are  $f_{0j} = [n(X_{gj})/(\pi^{3/2}v_{tj}^3)]\exp(-v^2/v_{tj}^2)$ , where  $v_{tj} = \sqrt{2T_j(X_{gj})/m_j}$ ,  $X_{gj} = x - v_y/\Omega_j$ , and  $\Omega_j = -q_j B/m_j c$ . Three fluctuating scalar fields are introduced:  $\tilde{\phi}$ ,  $\tilde{A}_{\parallel} (= \tilde{\mathbf{A}} \cdot \hat{b})$ , and  $\tilde{A}_2 (= (\tilde{\mathbf{A}} \times \hat{e}_{\perp}) \cdot \hat{b})$ , where all perturbed quantities have the form  $\tilde{p}(\mathbf{r}, t) = p(x)\exp(ik_y y - i\omega t)$ ,  $p(x) = 1/\sqrt{2\pi} \int p(k)\exp(ikx)dk$ ,  $\hat{e}_{\perp} = \mathbf{k}_{\perp}/|k_{\perp}|$ ,  $\mathbf{k}_{\perp} = k_y \hat{y} + k\hat{x}$ , and  $\hat{b} = \mathbf{B}/|B|$ . For the fluctuations with  $\omega \ll |\Omega_j|$  and  $k_{\perp} \lambda_d \ll 1$ , we have derived<sup>26</sup> the kinetic integral equations for arbitrary  $\beta$  value. Replacing the quasineutrality condition with Poisson's equation in the previous equations,<sup>26</sup> we get

$$\begin{aligned} & \frac{k_{\perp}^2}{2} \frac{\Omega_e^2}{\omega_{pe}^2} \hat{\phi}(k) + \sum_j \frac{Z_j T_e}{T_j} \\ & \times \left\{ \hat{\phi}(k) + \left( \frac{1}{2\pi} \right) \int dk' \int dx \exp[i(k' - k)x] \right. \\ & \times \left[ L_j(0,0,0,0) \hat{\phi}(k') + \frac{v_{tj}}{v_{te}} L_j \left( 0,1, \frac{1}{2}, 0 \right) \hat{A}_2(k') \right. \\ & \left. \left. + \frac{v_{tj}}{v_{te}} L_j(0,0,0,1) \hat{A}_{\parallel}(k') \right] \right\} = 0, \end{aligned} \quad (1)$$

$$\begin{aligned} & \hat{A}_2(k) - \sum_j \frac{\beta_j}{2\pi b_j} \left\{ \int dk' \int dx \exp[i(k' - k)x] \right. \\ & \times \left[ \frac{v_{te}}{v_{tj}} L_j \left( 1,0, \frac{1}{2}, 0 \right) \hat{\phi}(k') + L_j(1,1,1,0) \hat{A}_2(k') \right. \\ & \left. \left. + L_j \left( 1,0, \frac{1}{2}, 1 \right) \hat{A}_{\parallel}(k') \right] \right\} = 0, \end{aligned} \quad (2)$$

$$\begin{aligned} & \hat{A}_{\parallel}(k) - \sum_j \frac{\beta_j}{2\pi b_j} \left\{ \int dk' \int dx \exp[i(k' - k)x] \right. \\ & \times \left[ \frac{v_{te}}{v_{tj}} L_j(0,0,0,1) \hat{\phi}(k') + L_j \left( 0,1, \frac{1}{2}, 1 \right) \hat{A}_2(k') \right. \\ & \left. \left. + L_j(0,0,0,2) \hat{A}_{\parallel}(k') \right] \right\} = 0. \end{aligned} \quad (3)$$

Here,

$$\begin{aligned} & L_j(m,n,s,l) = \left( \frac{-q_j}{|q_j|} \right)^{m+n} \int_0^{+\infty} dt t^s \exp(-t) J_m(\sqrt{2b_j t}) \\ & \times J_n(\sqrt{2b'_j t}) \frac{\omega_{*j}}{\omega - \omega_{Dj} t} K_{lj}, \end{aligned} \quad (4)$$

$$\begin{aligned} & K_{0j} = \left( \frac{\omega}{\omega_{*j}} - 1 \right) [\xi_j Z(\xi_j)] - \eta \left[ \xi_j^2 + \left( \xi_j^2 - \frac{1}{2} \right) \xi_j Z(\xi_j) \right] \\ & - \eta(t-1) [\xi_j Z(\xi_j)], \end{aligned} \quad (5)$$

$$K_{1j} = \frac{k_{\parallel}}{|k_{\parallel}|} \xi_j \left[ K_{0j} + \left( \frac{\omega_0}{\omega_{*j}} - 1 \right) - \eta(t-1) \right], \quad (6)$$

$$K_{2j} = \frac{k_{\parallel}}{|k_{\parallel}|} \xi_j K_{1j}, \quad (7)$$

$$\omega_{*j} = (k_y T_j)/(\Omega_j m_j L_n), \quad \omega_{Dj} = -\omega_{*j} L_n/L_B,$$

$$\omega_{pe}^2 = 4\pi n e^2/m_e, \quad b_j = k_{\perp}^2 \rho_j^2/2, \quad b'_j = k_{\perp}^{\prime 2} \rho_j^2/2,$$

$$\rho_j = v_{tj}/\Omega_j, \quad \xi_j = (\omega - \omega_{Dj} t)/|k_{\parallel}| v_{tj},$$

$$k_{\parallel} = (x/L_s) k_y, \quad k_{\perp}^2 = k_y^2 + k^2, \quad k_{\perp}^{\prime 2} = k_y^2 + k^{\prime 2},$$

$Z_j = -q_j/e$ ,  $\hat{\phi} = \phi$ ,  $\hat{A}_2 = i v_{te} A_2/c$ ,  $\hat{A}_{\parallel} = -v_{te} A_{\parallel}/c$ , and  $Z(\xi)$  is the plasma dispersion function.

We call Eqs. (1)–(3) full  $\beta$  model as in the previous work.<sup>26</sup> When the coupling to the compressional Alfvén waves (CAWs) and the magnetic gradient effects are omitted, that is,  $\hat{A}_2 = 0$  and  $L_B \rightarrow \infty$ , we get the low  $\beta$  model.

## III. LOCAL ANALYSIS

We first consider the local modes in the electrostatic limit, that is, we take  $k = k' = 0$ ,  $k_{\parallel} = \text{const}$  and  $\beta = 0$ . The Debye shielding effect,  $\Omega_e^2/\omega_{pe}^2$ , is also neglected. The simplified dispersion equation is the same as the electrostatic limit of the dispersion equation in Smolyakov *et al.*,<sup>23</sup>

$$D_e + \tau D_i = 0, \tag{8}$$

where

$$D_j = 1 - \eta_j \frac{\omega \omega_{*j}}{k_{\parallel}^2 v_{tj}^2} \Gamma(b_j) + \left\{ 1 - \frac{\omega_{*j}^T}{\omega} - \eta_j \frac{\omega_{*j}}{\omega} \right. \\ \left. \times \left[ 1 - b_j \left( 1 - \frac{I_{1j}}{I_{0j}} \right) \right] \right\} \Gamma(b_j) \frac{\omega}{k_{\parallel} v_{tj}} Z \left( \frac{\omega}{k_{\parallel} v_{tj}} \right), \tag{9}$$

and  $\omega_{*j}^T = \omega_{*j} [1 - \eta_j (3/2 - \omega^2/\omega_{tj}^2)]$ . When the quasifluid assumption,  $v_{te} > |\omega|/k_{\parallel} \approx v_{ti}$ , is valid, we can neglect the terms of order  $(k_{\parallel}^2 v_{ti}^2/\omega^2)$  and order  $(\omega^2/k_{\parallel}^2 v_{te}^2)$  and get

$$D_i = 1 - \Gamma_{0i} + \frac{\omega_{*i}}{\omega} (1 - \eta_i \varepsilon_i) \Gamma_{0i} \\ + i \pi^{1/2} \frac{\omega}{k_{\parallel} v_{ti}} \exp \left( - \frac{\omega^2}{k_{\parallel}^2 v_{ti}^2} \right) \Gamma_{0i} \delta_i, \tag{10}$$

$$D_e = 1 + \frac{2 \omega_{*e} \omega}{k_{\parallel}^2 v_{te}^2} [1 - \eta_e - \eta_e \varepsilon_e] \Gamma_{0e} + i \pi^{1/2} \frac{\omega}{k_{\parallel} v_{te}} \Gamma_{0e} \delta_e, \tag{11}$$

with

$$\delta_i = 1 - \frac{\omega_{*i}}{\omega} \left( 1 - \frac{\eta_i}{2} - \eta_i \varepsilon_i + \eta_i \frac{\omega^2}{k_{\parallel}^2 v_{ti}^2} \right), \tag{12}$$

$$\delta_e = 1 - \frac{\omega_{*e}}{\omega} \left( 1 - \frac{\eta_e}{2} - \eta_e \varepsilon_e \right), \tag{13}$$

and

$$\varepsilon_j = b_j \left[ 1 - \frac{I_{1j}(b_j)}{I_{0j}(b_j)} \right]. \tag{14}$$

For weakly growing modes,  $\gamma < \omega_r$ , we obtain

$$\frac{\omega_r}{k_{\parallel} v_{ti}} = - \frac{(\sqrt{b_i/2}/k_{\parallel} L_n)(\eta_i \varepsilon_i - 1) \Gamma_{0i}}{2 - \Gamma_{0i} + 2(m_e/m_i)(\sqrt{b_i/2}/k_{\parallel} L_n)(\omega_r/k_{\parallel} v_{ti})(1 - \eta_e - \eta_e \varepsilon_e)}, \tag{15}$$

$$\frac{\gamma}{k_{\parallel} v_{ti}} = \frac{\pi^{1/2}}{(\sqrt{b_i/2}/k_{\parallel} L_n)(\eta_i \varepsilon_i - 1) \Gamma_{0i}} \left( \frac{\omega_r^3}{k_{\parallel}^3 v_{ti}^3} \right) \\ \times \left[ \exp \left( - \frac{\omega_r^2}{k_{\parallel}^2 v_{ti}^2} \right) \Gamma_{0i} \delta_i + \sqrt{\frac{m_e}{m_i}} \Gamma_{0e} \delta_e \right]. \tag{16}$$

Here, the assumption  $\tau=1$  and the relation  $\omega_{*j}/k_{\parallel} v_{tj} = \sqrt{b_j/2}/k_{\parallel} L_n$  are used.

The real frequency is nonmonotonic mostly because of the nonmonotonic behavior of  $b_j^r \varepsilon_j$  as  $b_j$  varies, where  $r$  is a rational number. The maximum value of the real frequency,  $(\omega_r/k_{\parallel} v_{ti})_{\max}$ , mostly depends on  $\eta_i$  and  $k_{\parallel} L_n$ . The growth rate  $\gamma$  is principally decided by the  $\omega_r$  in the form of  $(\omega_r/k_{\parallel} v_{ti})^m \exp(-\omega_r^2/k_{\parallel}^2 v_{ti}^2)$ . The initial rise in real frequency, from below to above  $(\omega_r/k_{\parallel} v_{ti})_c$ , causes an increase in  $\gamma$ . As  $\omega_r/k_{\parallel} v_{ti} \geq (\omega_r/k_{\parallel} v_{ti})_c$ , a further increase in real frequency will cause a decrease in  $\gamma$ . If  $(\omega_r/k_{\parallel} v_{ti})_{\max} < (\omega_r/k_{\parallel} v_{ti})_c$ , there is only one peak in the relation of  $\gamma$  vs  $b_i$ , corresponding to the maximum frequency. If  $\eta_i$  is large enough,  $(\omega_r/k_{\parallel} v_{ti})_{\max} \geq (\omega_r/k_{\parallel} v_{ti})_c$ , there will be a ‘‘double-hump’’ behavior in the spectrum of  $\gamma$  vs  $b_i$ . The first peak in the regime  $b_i \lesssim 1$  is called the conventional ITG mode. The second peak is just the short wavelength ITG mode mentioned in Smolyakov *et al.*<sup>23</sup> The mode frequency and growth rate as functions of  $b_i$  are shown in Fig. 1 for different  $\eta_i$  values at  $k_{\parallel} L_n = 0.1$  and  $\eta_e = 4.6$ . When the maximum frequency decreases with  $\eta_i$ , the  $\gamma$  turns out to have a hump once as  $b_i$  varies. Smolyakov *et al.*<sup>23</sup> also gave a similar plot, but they explained it as the disappearance of the second peak at low  $\eta_i$ .

In fact, Pu and Migliuolo<sup>24</sup> pointed out the ‘‘double-hump’’ behavior correctly. However, the second peak in their results is slight and not clear. One reason is that the parallel

wave number used in the work is so much larger,  $k_{\parallel} L_n = 0.2$ , that  $(\omega_r/k_{\parallel} v_{ti})_{\max}$  is very small. The other reason is that the electron temperature gradient effect is not taken into account, that is,  $\eta_e = 0$  is assumed in that work. We find that

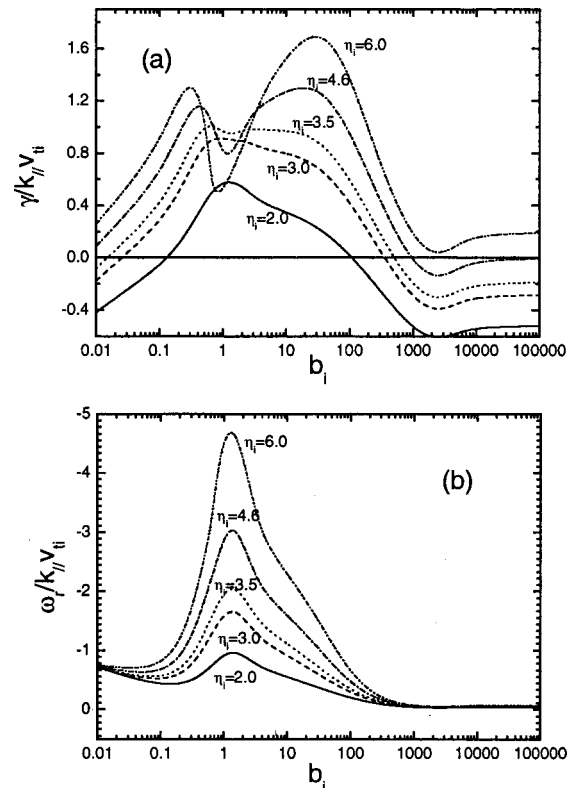


FIG. 1. Normalized growth rate (a) and frequency (b) of the local modes as functions of  $b_i$  for  $\eta_i = 2, 3, 3.5, 4.6,$  and  $6$ , respectively. The other parameters are  $\beta=0$ ,  $m_i/m_e = 1836$ ,  $T_e/T_i = 1$ ,  $k_{\parallel} L_n = 0.1$ , and  $\eta_e = 4.6$ .

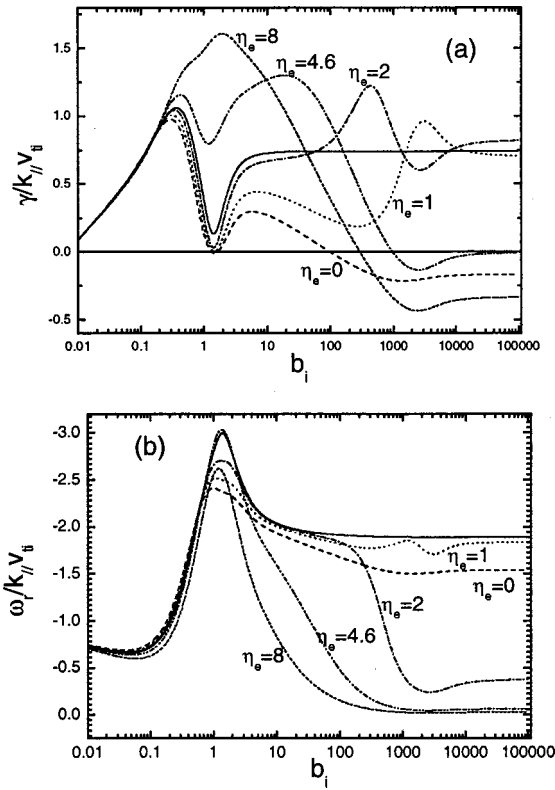


FIG. 2. The same as in Fig. 1 except that  $\eta_i=4.6$  and  $\eta_e=0, 1, 2, 4.6,$  and  $8$ , respectively, here. The solid lines denote the results from the model with adiabatic electrons.

electron kinetics strongly influences the behavior of the modes in the short wavelength regime. The  $k_y$  spectrum of the modes is presented in Fig. 2 for different  $\eta_e$ . The abundant behaviors of the modes can be explained qualitatively, or even quantitatively from the following analytical analyses of Eqs. (8)–(16).

If the electrons are adiabatic, the real frequency and growth rate tend to certain constant values for  $b_i \gg 1$ . It is because  $\lim_{b_i \rightarrow +\infty} \Gamma_{0i} = (2\pi b_i)^{-1/2}$  and  $\lim_{b_i \rightarrow +\infty} \varepsilon_i = 1/2$ . However, electrons become more effective as  $b_i$  increases. First, the electron Landau damping can directly influence the growth rate in Eq. (16). For  $\omega/k_{\parallel}v_{ti} > 1$ ,  $b_i \gg 1$  and  $b_e < 1$ , the electron contribution to the growth rate  $\sqrt{m_i/m_e}\Gamma_{0e}\delta_e$  is comparable to the ion contribution  $\exp(-\omega^2/k_{\parallel}^2v_{ti}^2)\Gamma_{0i}\delta_i$ . The electron response may be stabilizing or destabilizing, depending on the sign of the  $\delta_e$ . Moreover, a large  $\eta_e$  tends to decrease the real frequency when the term  $2(m_e/m_i) \times (\sqrt{b_i/2}/k_z L_n)(\omega_r/k_{\parallel}v_{ti})(\eta_e + \eta_e \varepsilon_e - 1)$  is of the order of unity.

At a very small  $\eta_e (< 0.4)$ , the mode is unstable in the regime  $b_e \ll 1$  and stable in the very short wavelength regime  $b_e \gg 1$ . Moreover, the second peak of the growth rate is slightly smaller than the first peak, which is similar to the results in Pu and Migliuolo.<sup>24</sup> This is because  $\delta_e$  is always stabilizing for very small  $\eta_e$ . Also, a small  $\eta_e$  hardly changes the real frequency. The destabilizing  $\delta_i$  is constant in this parameter region. If the electron stabilizing effect is stronger than the ion destabilizing effect, the mode is fully stabilized.

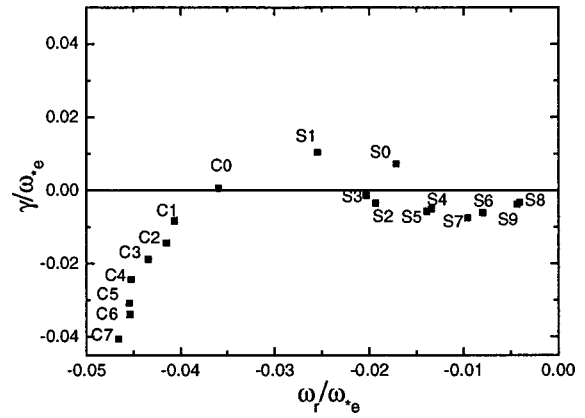


FIG. 3. The eigenvalues of the nonlocal modes for  $k_y \rho_e = 0.1$ ,  $\beta = 0$ ,  $m_i/m_e = 1836$ ,  $T_e/T_i = 1$ ,  $L_s/L_n = 0.025$ , and  $\eta_i = \eta_e = 2$ . The letters, C and S denote different series and the numbers denote different harmonic orders.

If  $\eta_e$  is about 1, the  $\delta_e$  is stabilizing in the small  $b_e$  regime and destabilizing in the large  $b_e$  regime. So the growth rate decreases first and then increases as  $\delta_e$  increases. Since  $\delta_i$  is constant at large  $b_i$ , the growth rate reaches its minimum at certain value of  $\delta_e$ , namely  $\delta_{em}$ , where  $\partial\delta_e/\partial b_e = 0$ . Under the assumption of  $b_e < 1$ ,  $\delta_e \sim \sqrt{b_e}(1 - \eta_e/2 - \eta_e b_e)$ , so  $\partial\delta_e/\partial b_e = 0$  gives  $b_{em} = (2 - \eta_e)/6\eta_e$ . For  $\eta_e = 1$ , the corresponding  $b_{em}$  is 0.167, that is,  $b_i \sim 300$ . It is well consistent with the numerical result.

When  $\eta_e > 2$ ,  $\delta_e < 0$ , then the electron contribution is always destabilizing. The growth rate is increased by both of the ion and electron destabilizing effects when  $\omega/k_{\parallel}v_{ti} > 1$ . However, the real frequency decreases as  $b_i$  increases. When the  $\omega/k_{\parallel}v_{ti}$  approaches to 1, the sign of  $\delta_i$  in Eq. (12) reverses, that is, the ion response becomes stabilizing. Moreover,  $\exp(-\omega^2/k_{\parallel}^2v_{ti}^2)\Gamma_{0i}\delta_i$  is much larger than  $\sqrt{m_i/m_e}\Gamma_{0e}\delta_e$  for  $\omega/k_{\parallel}v_{ti} \sim 1$ . Since the ion stabilizing effect becomes dominant, the growth rate consequently decreases. So the second hump occurs around  $\omega/k_{\parallel}v_{ti} \sim 1$ . Strictly speaking, the analysis based on the fluid assumption breaks down in that case. However, we can roughly estimate a scaling law of  $b_i$  and  $\eta_e$  corresponding to these second peaks in Fig. 2. That is,  $\sqrt{b_i}(\eta_e - 1) = \text{const}$ . When  $\eta_e$  increases to very large values, the second peak moves toward the long wavelength regime and then joins with the first peak. When  $b_e$  is also much larger than 1, the real frequency and growth rate tend to be constant, since  $\Gamma_{0i}\omega_{*i}/k_{\parallel}v_{ti} = -\Gamma_{0e}\omega_{*e}/k_{\parallel}v_{te} = \text{const}$ . Consequently, the electron effects decrease the real frequency to a very low level. With  $\omega/k_{\parallel}v_{ti} < 1$ , the dispersion equation becomes

$$2 + \frac{2\omega_{*i}\omega}{k_{\parallel}^2 v_{ti}^2} \Gamma_{0i} \left[ 1 - \frac{3}{2} \eta_i - \frac{v_{ti}}{v_{te}} \left( 1 - \frac{3}{2} \eta_e \right) \right] + i\pi^{1/2} \frac{\omega_{*i}}{k_{\parallel} v_{ti}} \Gamma_{0i} (\eta_i - \eta_e) = 0, \tag{17}$$

then

$$\frac{\omega_r}{k_{\parallel} v_{ti}} = \frac{k_{\parallel} v_{ti}}{\omega_{*i} \Gamma_{0i}} \left/ \left[ \frac{3}{2} \eta_i - 1 + \frac{v_{ti}}{v_{te}} \left( \frac{3}{2} \eta_e - 1 \right) \right] \right., \tag{18}$$

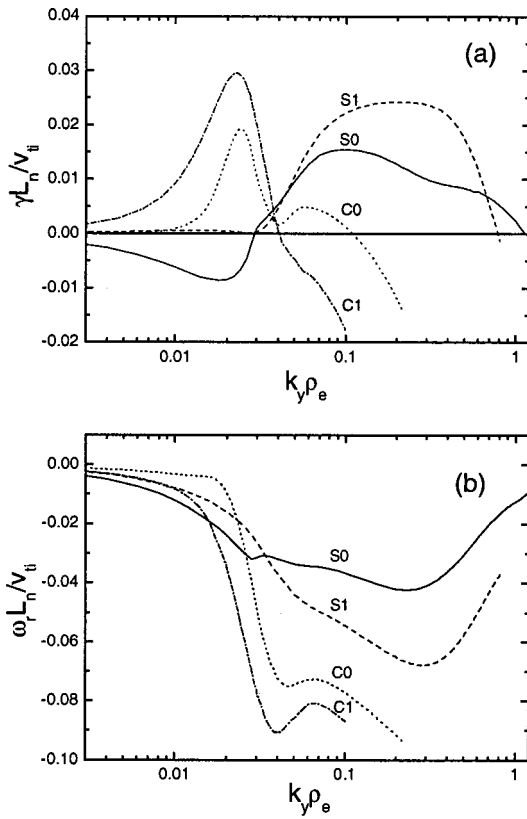


FIG. 4. Normalized growth rate (a) and frequency (b) of the nonlocal modes as functions of  $k_y\rho_e$  for  $\beta=0$ ,  $m_i/m_e=1836$ ,  $T_e/T_i=1$ ,  $L_s/L_n=0.025$ , and  $\eta_i=\eta_e=2$ . The solid, dashed, dotted, and dashed-dotted lines denote the S0, S1, C0, and C1 modes, respectively.

$$\frac{\gamma}{k_{\parallel}v_{ti}} = \frac{\pi^{1/2}}{2}(\eta_i - \eta_e) \left/ \left[ \frac{3}{2}\eta_i - 1 + \frac{v_{ti}}{v_{te}} \left( \frac{3}{2}\eta_e - 1 \right) \right] \right. \quad (19)$$

Therefore, a large  $\eta_e (> \eta_i)$  can fully stabilize the mode in the very short wavelength regime of  $b_e > 1$ . The analytic result is in good agreement with the numerical results shown in Fig. 2.

IV. NONLOCAL ANALYSIS

In the nonlocal model, the parallel wave number,  $k_{\parallel} = (x/L_s)k_y$ , is related to the mode structure and the cross-field wave number,  $k_{\perp} = \sqrt{k_y^2 + k^2}$ , includes poloidal and radial components. Then, there may exist several distinctive modes with different structures in different frequency regions. In the long wavelength regime  $|k_y\rho_i| \leq 1$ , in fact, the conventional ITG modes with different orders have been identified and investigated.<sup>3,27,28</sup> In this paper, we will identify a new series of short wavelength modes. For the nonlocal mode, we only set the  $k_y$ , whereas the  $k_x$  spectrum is determined by the solutions to the eigenmode equations. On the other hand, a high  $\eta_i$  is not needed to destabilize the short wavelength mode, since the mode structure can be adjusted to make  $\omega/k_{\parallel}v_{ti}$  large enough. In the following calculations, we choose the parameters:  $\eta_e=2$ ,  $\eta_i=2$ ,  $T_e/T_i=1$ ,  $m_i/m_e=1836$ ,  $L_n/L_s=0.025$ , and  $k_y\rho_e=0.1$ , unless otherwise stated. The ion and electron temperature gradient parameters employed are the usual ones seen in previous studies of conventional ITG modes.<sup>3,26-28</sup> The poloidal wavelength employed is close to that in Hirose *et al.*,<sup>25</sup> where  $|k_y\rho_i|=6$ .

Shown in Fig. 3 are the eigenvalues of the dispersion equations for  $k_y\rho_e=0.1$ , i.e., S0, S1, C0, C1, and so on, in the complex plane of the frequency normalized to  $\omega_{*e}$ . The letter, C or S, denotes a different series of the branch of the modes. The even and odd numbers denote the even and odd modes, respectively. The mode structure becomes more com-

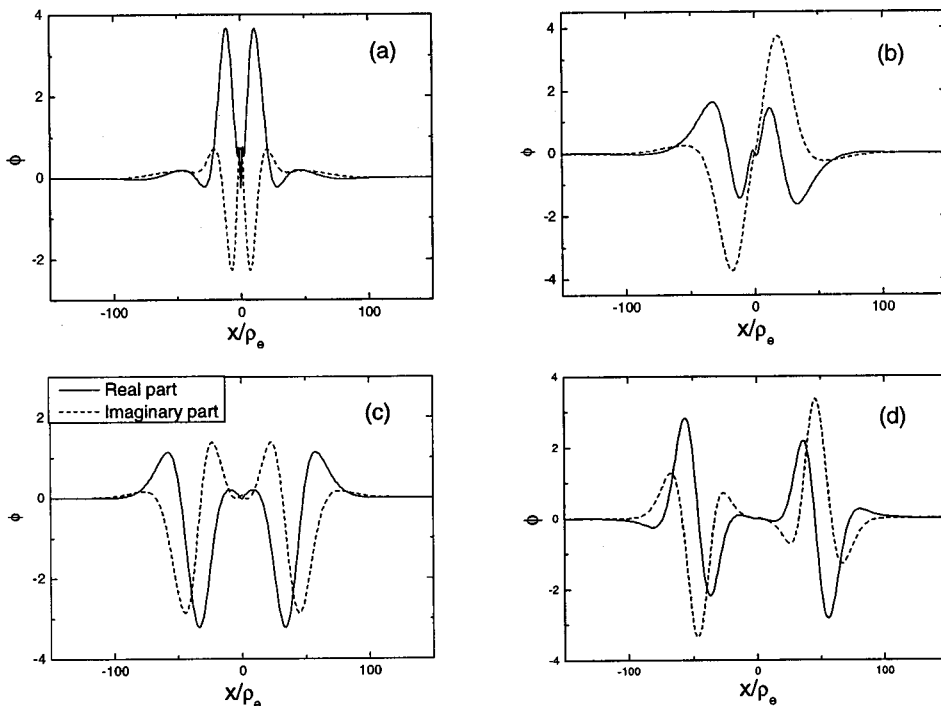


FIG. 5. Mode structures of the S0 (a), S1 (b), C0 (c), and C1 (d) modes for  $k_y\rho_e=0.1$ . The parameters are the same as in Fig. 3.

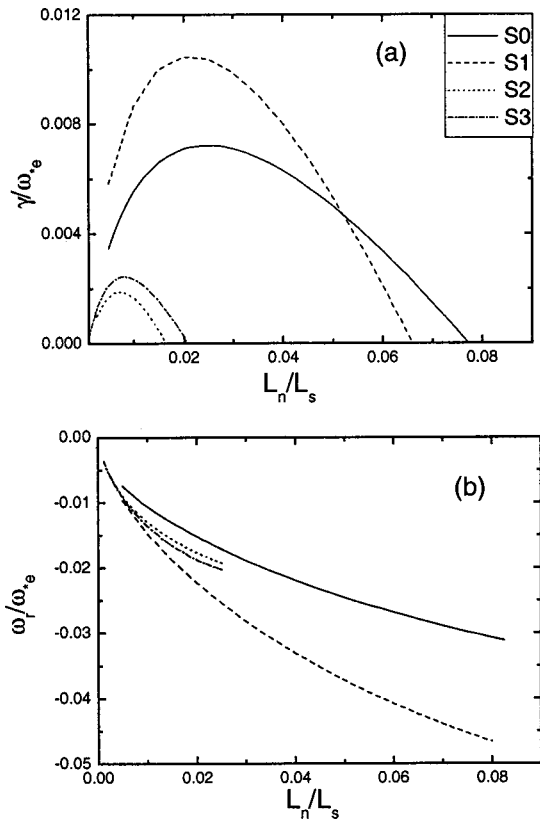


FIG. 6. Normalized growth rate (a) and frequency (b) as functions of  $L_s/L_n$  for the S0 (the solid lines), S1 (the dashed lines), S2 (the dotted lines), and S3 (the dashed-dotted lines) modes, respectively. The other parameters are the same as in Fig. 3.

plicated as the number increases. The solutions with higher frequencies, the C series, seem to be on the short wavelength tail of the conventional ITG modes, e.g., the C0, C1, and C2 are verified to be the conventional ITG modes at  $k_y \rho_e = 0.1$  with the harmonic order number  $l = 0, 1,$  and  $2,$  respectively. However, only the fundamental mode is unstable in the short wavelength regime. The higher order modes are rather stable. The other solutions with lower frequencies, the S series, are considered to be short wavelength modes. The  $k_y$  spectra of the lowest even and odd short wavelength modes are shown in Fig. 4, along with those for the lowest even and odd conventional ITG modes. The index C0, C1, S0, and S1 characterizing these modes are also marked in Fig. 4 and the corresponding mode structures are shown in Fig. 5. The growth rate of the unstable modes reaches the maximum value at short wavelength regions. Although the wavelengths in y-direction are short, the radial widths of the modes can be comparable with those of the conventional ITG modes, and much larger than those of the ETG modes.

Similar with the conventional ITG mode, the higher order short wavelength mode is unstable only in case of very weak magnetic shear. In other words, the higher order mode is more easily stabilized by magnetic shear. The magnetic shear stabilization of the S0, S1, S2, and S3 modes are shown in Fig. 6. Not shown in the figure is that the higher order modes, S4 and S5, are unstable at much weaker mag-

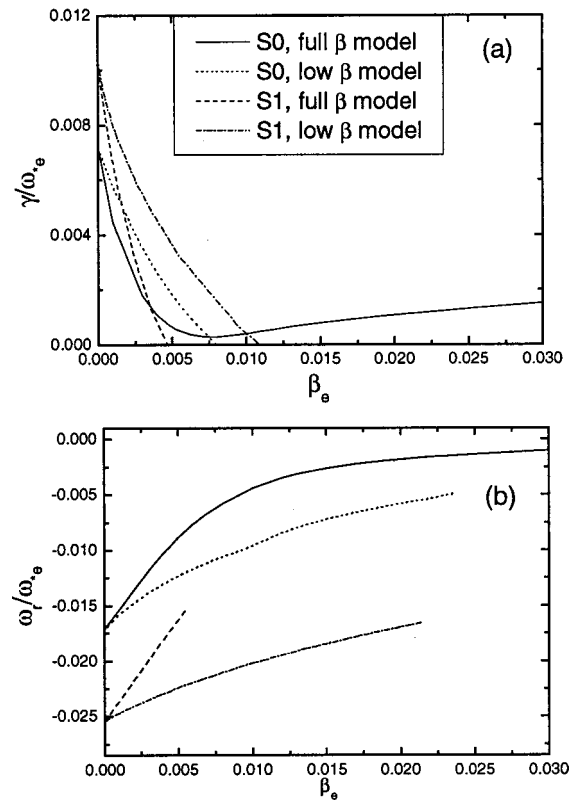


FIG. 7. Normalized growth rate (a) and frequency (b) as functions of  $\beta_e$ . Solid lines: the S0 mode from the full  $\beta$  model; dashed lines: the S1 mode from the full  $\beta$  model; dotted lines: the S0 mode from the low  $\beta$  model; dashed-dotted lines: the S1 mode from the low  $\beta$  model. The other parameters are the same as in Fig. 3.

netic shear regions, and that the S6 and S7 modes are almost always stable.

From Fig. 6, we see that the S1 mode, the lowest odd mode, is more easily stabilized by magnetic shear than the S0 mode, although the S1 mode has a higher growth rate at weak magnetic shear. The same is true for finite  $\beta$  stabilization. Shown in Fig. 7 are the frequencies and growth rates of the S0 and S1 modes as functions of  $\beta_e$ , obtained from the low  $\beta$  and full  $\beta$  models. The S1 mode may be stabilized by a finite  $\beta$  in both of the models. The fundamental mode cannot be stabilized by  $\beta$  when the magnetic gradient effect is considered in the full  $\beta$  model. Therefore, the S1 mode is more unstable at low  $\beta$  and weak magnetic shear regions than the fundamental mode, while the latter is dominant in tokamak-type plasmas where low shear regimes usually exist in the interior with high  $\beta$ . A similar conclusion was reached for the conventional ITG modes.<sup>28</sup>

There is an obvious difference between the local and nonlocal results. The frequency of the local mode is continuous as  $b_i$  varies, while the conventional mode and the short wavelength mode are separated, as shown in Fig. 4. However, the conventional and short wavelength modes couple to each other when  $\eta_e$  increases. Figure 8 shows the  $k_y$  spectra of the modes at a higher value of  $\eta_e (= 4)$ . The coupling results in a continuous  $k_y$  spectrum with two humps in the short wavelength and long wavelength regimes, respectively. The coupling also introduces another series with lower

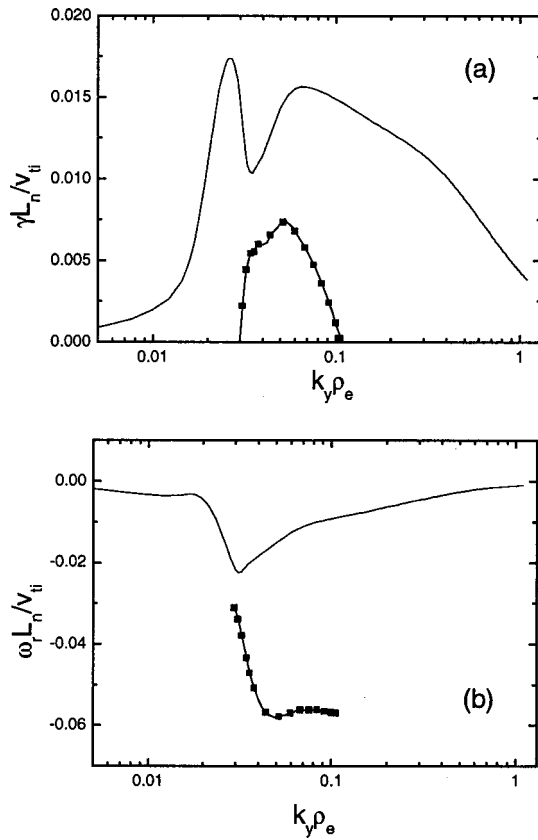


FIG. 8. Normalized growth rate (a) and frequency (b) of the nonlocal modes as functions of  $k_y \rho_e$  for  $\eta_e = 4$ . The solid lines denote the dominant mode and the lines with squares denote the other weak growing mode due to the coupling between the fundamental short wavelength mode and the conventional mode.

growth rate in the medium wavelength regime, which is shown in Fig. 8 by the lines with squares.

When  $\beta$  increases, a similar coupling occurs. Shown in Fig. 9 are the  $k_y$  spectra for  $\beta_e = 0.001, 0.005,$  and  $0.05$ , respectively. For  $\beta_e = 0.001$ , the series with lower frequency and higher growth rate in Fig. 9 may correspond to the nonlocal toroidal mode at finite beta found by Hirose *et al.*<sup>25</sup> Accompanying this dominant mode, a novel mode with higher frequency and lower growth rate is unstable in the medium wavelength regime. This mode is fully suppressed at higher  $\beta$ . So, there is only one continuous mode in high  $\beta$  plasmas. This mode is just the same as the high  $\beta$  ITG mode we studied earlier.<sup>26</sup>

Hirose *et al.*<sup>25</sup> indicates that both finite  $\eta_i$  and  $\eta_e$  are required for the excitation of the toroidal short wavelength mode. Here, the slab mode also requires finite  $\eta_i$  and  $\eta_e$ . The normalized growth rate,  $\gamma/\omega_{*e}$ , vs  $\eta_e$  for fixed  $\eta_i$  and  $\gamma/\omega_{*e}$  vs  $\eta_i$  for fixed  $\eta_e$  are shown in Figs. 10(a) and 10(b), respectively. In Hirose *et al.*,<sup>25</sup> the magnetic shear has destabilizing effects on the toroidal modes. However, in a slab configuration, a large enough magnetic shear stabilizes the short wavelength modes, although the growth rates increase with the shear parameter at very weak shear regions. It is shown in Fig. 11(a) that the stabilizing effect of magnetic shear is also effective at finite  $\beta$ . The real frequency increases with the magnetic shear. This dependence of the fre-

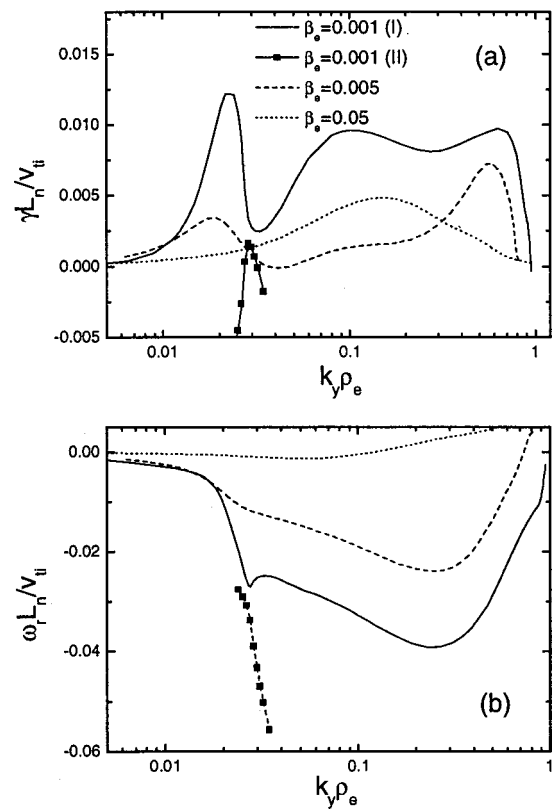


FIG. 9. Normalized growth rate (a) and frequency (b) of the nonlocal modes as functions of  $k_y \rho_e$  for  $\beta_e = 0.001$  (the solid lines),  $0.005$  (the dashed lines), and  $0.05$  (the dotted lines). The weak-growing mode due to the coupling between the fundamental short wavelength mode and the conventional mode for  $\beta_e = 0.001$  (the lines with squares) vanishes as  $\beta_e$  increases.

quency on the shear parameter may be attributed to ion/electron transit frequency  $k_{\parallel} v_i$ . However, the growth rate increases first and decreases finally as the real frequency increases.

For short wavelength modes, the Debye shielding effect is usually important. For example, the Debye shielding has a clear stabilization effect on the ETG mode.<sup>22</sup> Shown in Fig. 11(b) is the Debye shielding effect on the short wavelength modes. The Debye shielding parameter  $\Omega_e^2/\omega_{pe}^2$  with order unity can suppress the mode, especially in short wavelength regions, but cannot fully stabilize the mode.

### V. CONCLUSIONS

In this paper, the short wavelength ion mode driven by temperature gradients is studied in a sheared slab. The local short wavelength mode is attributable to the Landau damping/inverse Landau damping mechanism and the non-monotonic behaviors of the real frequency with wavelength variation. When  $\eta_i$  is large enough, the growth rate has the humps in both the long wavelength regime  $|k_y \rho_i| \leq 1$  and the short wavelength regime  $|k_y \rho_i| > 1$ . The electron temperature gradient strongly influences the properties of the modes in the short wavelength regions. The mode behaves differently for different electron temperature gradient. The mode is stable in the very short wavelength regime  $k_y \rho_e \gtrsim 1$  for  $\eta_e$  value very small ( $\ll 1$ ) or larger than  $\eta_i$  only.

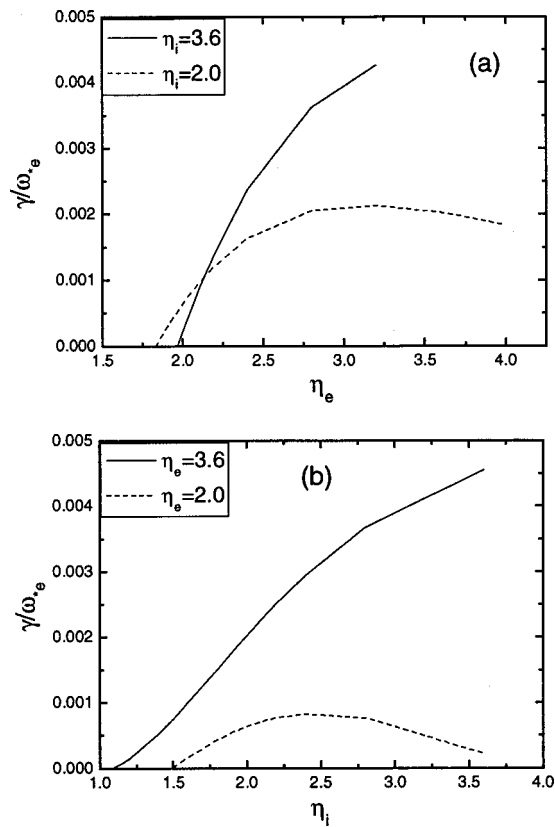


FIG. 10. Normalized growth rate of the fundamental short wavelength mode as functions of  $\eta_e$  (a) and  $\eta_i$  (b) for  $\beta_e = 0.005$ , respectively. The other parameters are the same in Fig. 3.

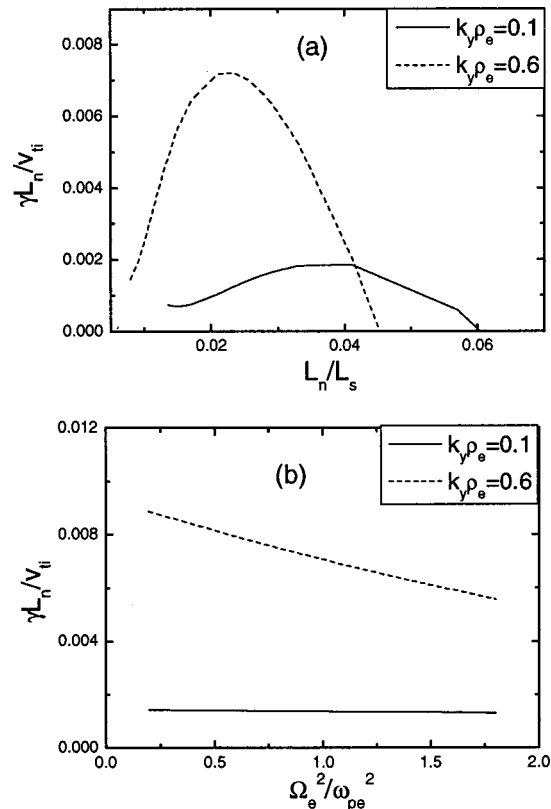


FIG. 11. Normalized growth rate of the fundamental short wavelength mode as functions of  $L_n/L_s$  (a) and  $\Omega_e^2/\omega_{pe}^2$  (b) for  $\beta_e = 0.005$  and  $k_y \rho_e = 0.1$  (the solid lines) and 0.6 (the dashed lines), respectively. The other parameters are the same as in Fig. 3.

From the integral eigenmode equations, we have also identified a series of eigenmodes in the short wavelength regime. Although the lowest odd mode has a higher growth rate in low  $\beta$  and weak magnetic shear regions, the fundamental mode, i.e., the lowest even mode, seems to be important in tokamak-type plasmas. The fundamental mode cannot be stabilized by  $\beta$ , but can be stabilized by magnetic shear. However, the higher order modes are easily stabilized by magnetic shear and by finite  $\beta$ . The short wavelength mode is separate from the conventional ITG mode in some parameter regimes. However, the coupling occurs between these two series when the  $\beta$  or  $\eta_e$  increases. Then the dominant mode has a continuous  $k_y$  spectrum from long wavelength to short wavelength regions, which is similar to the short wavelength mode in the toroidal geometry. Although the poloidal wavelength is short, the radial width of the mode is found to be comparable with that of the conventional ITG mode and much larger than that of the ETG mode. Both  $\eta_i$  and  $\eta_e$  over the threshold are required for the excitation of unstable modes. The Debye shielding effect can compress the mode but cannot fully stabilize the mode.

**ACKNOWLEDGMENTS**

The useful discussion with Dr. H. Sugama on the ITG mode is gratefully acknowledged. The authors also wish to thank Dr. M. Yagi for the discussion of the short wavelength instabilities.

One of the authors (Z.G.) is grateful for the hospitality by many staff members during his visit at the National Institute for Fusion Science, Japan. This work is supported by the JSPS-CAS (Japan–China) Core University Program on Plasma and Nuclear Fusion, by Improving Tsinghua to Top-ranking University Fund and by National Science Foundation of China, Grants Nos. 19889506 and 10135020. This work is partly supported by the Grant-in-Aid for Scientific Research of MEXT, Japan.

<sup>1</sup>K. Itoh and S.-I. Itoh, Plasma Phys. Controlled Fusion **38**, 1 (1996).  
<sup>2</sup>B. Coppi, M. N. Rosenbluth, and R. Z. Sagdeev, Phys. Fluids **10**, 582 (1967).  
<sup>3</sup>R. Linsker, Phys. Fluids **24**, 1485 (1981).  
<sup>4</sup>Y. C. Lee, J. Q. Dong, P. N. Guzdar, and C. S. Liu, Phys. Fluids **30**, 1331 (1987).  
<sup>5</sup>A. Jarmen, P. Anderson, and J. Weiland, Nucl. Fusion **27**, 941 (1987).  
<sup>6</sup>W. Horton, B. G. Hong, and W. M. Tang, Phys. Fluids **31**, 2971 (1988).  
<sup>7</sup>T. S. Hahm and W. M. Tang, Phys. Fluids B **1**, 1185 (1989).  
<sup>8</sup>L. Chen, S. Briguglio, and F. Romanelli, Phys. Fluids B **3**, 611 (1991).  
<sup>9</sup>J. Y. Kim, W. Horton, and J. Q. Dong, Phys. Fluids B **5**, 4030 (1993).  
<sup>10</sup>M. A. Beer and G. W. Hammett, Phys. Plasmas **3**, 4046 (1996).  
<sup>11</sup>W. W. Lee and R. A. Santoro, Phys. Plasmas **4**, 169 (1997).  
<sup>12</sup>F. M. Levinton, M. C. Zarnstorff, S. H. Batha, M. Bell, R. E. Bell, R. V. Budny, C. Bush, Z. Chang, E. Fredrickson, A. Janos, J. Manickam, A. Ramsey, S. A. Sabbagh, G. L. Schmidt, E. J. Synakowski, and G. Taylor, Phys. Rev. Lett. **75**, 4417 (1995).  
<sup>13</sup>H. Shirai and JT-60 Team, Phys. Plasmas **5**, 1712 (1998).  
<sup>14</sup>S.-I. Itoh and K. Itoh, Phys. Rev. Lett. **60**, 2276 (1988).  
<sup>15</sup>E. Mazzuato, S. H. Batha, M. Beer, R. E. Bell, R. V. Budny, C. Bush, T. S. Hahm, G. W. Hammett, F. M. Levinton, R. Nazikian, H. Park, G. Rewoldt, G. L. Schmidt, E. J. Synakowski, W. M. Tang, G. Taylor, and M. C. Zarnstorff, Phys. Rev. Lett. **77**, 3145 (1996).

- <sup>16</sup>K. H. Burrell, *Phys. Plasmas* **4**, 1499 (1997).
- <sup>17</sup>Z. Lin, T. S. Hahm, W. W. Lee, W. M. Tang, and R. B. White, *Science* **281**, 1835 (1998).
- <sup>18</sup>P. Beyer, S. Benkadda, X. Garbet, and P. H. Diamond, *Phys. Rev. Lett.* **85**, 4892 (2000).
- <sup>19</sup>G. D. Conway, D. N. Borba, B. Alper, D. V. Bartlett, C. Gormezano, M. G. von Hellermann, A. C. Maas, V. V. Parail, P. Smeulder, and K.-D. Zastrow, *Phys. Rev. Lett.* **84**, 1463 (2000).
- <sup>20</sup>Y. Idomura, M. Wakatani, and S. Tokuda, *Phys. Plasmas* **7**, 2456 (2000).
- <sup>21</sup>F. Jenko, W. Dorlanf, M. Kotschenreuther, and B. N. Rogers, *Phys. Plasmas* **7**, 1904 (2000).
- <sup>22</sup>J. Q. Dong, H. Sanuki, and K. Itoh, *Phys. Plasmas* **8**, 3635 (2001).
- <sup>23</sup>A. I. Smolyakov, M. Yagi, and Y. Kishimoto, *Phys. Rev. Lett.* **89**, 125005 (2002).
- <sup>24</sup>Y.-K. Pu and S. Migliuolo, *Phys. Fluids* **28**, 1722 (1985).
- <sup>25</sup>A. Hirose, M. Elia, A. I. Smolyakov, and M. Yagi, *Phys. Plasmas* **9**, 1659 (2002).
- <sup>26</sup>Z. Gao, J. Q. Dong, G. J. Liu, and C. T. Ying, *Phys. Plasmas* **9**, 569 (2002).
- <sup>27</sup>J. V. M. Reynders, *Phys. Plasmas* **1**, 1953 (1994).
- <sup>28</sup>Z. Gao, J. Q. Dong, G. J. Liu, and C. T. Ying, *Phys. Plasmas* **9**, 1692 (2002).